Engineering Geology 127 (2012) 14–26

Contents lists available at SciVerse ScienceDirect

Engineering Geology

journal homepage: www.elsevier.com/locate/enggeo

Spatial distribution of landslides triggered from the 2007 Niigata Chuetsu–Oki Japan Earthquake

Brian D. Collins [a,*], Robert Kayen [b,1], Yasuo Tanaka [c,2]

[a] U.S. Geological Survey, Western Earth Surface Processes Team, 345 Middlefield Road, MS973, Menlo Park, CA 94025, USA
[b] U.S. Geological Survey, Coastal and Marine Geology Team, 345 Middlefield Road, MS999, Menlo Park, CA 94025, USA
[c] Kobe University, Research Center for Urban Safety and Security, Nada, Kobe 657-8501, Japan

ARTICLE INFO

Article history:
Received 12 April 2011
Received in revised form 29 November 2011
Accepted 3 December 2011
Available online 2 January 2012

Keywords:
Landslide
Earthquake
Kashiwazaki
Japan
Coastal
Ground motion

ABSTRACT

Understanding the spatial distribution of earthquake-induced landslides from specific earthquakes provides an opportunity to recognize what to expect from future events. The July 16, 2007 M_w 6.6 (M_{JMA} 6.8) Niigata Chuetsu–Oki Japan earthquake triggered hundreds of landslides in the area surrounding the coastal city of Kashiwazaki and provides one such opportunity to evaluate the impacts of an offshore, magnitude 6+ earthquake on a steep coastal region. As part of a larger effort to document all forms of geotechnical damage from this earthquake, we performed landslide inventory mapping throughout the epicentral area and analyzed the resulting data for spatial, seismic-motion, and geologic correlations to describe the pattern of landsliding. Coupled with examination of a third-party, aerial-photo-based landslide inventory, our analyses reveal several areas of high landslide concentration that are not readily explained by either traditional epicentral and fault–plane-distance metrics or by recorded and inferred ground-motions. Whereas average landslide concentrations averaged less than 1 landslide per square kilometer (LS/km^2), some areas reached up to 2 LS/km^2 in the Nishiyama Hills to the northeast of Kashiwazaki and between 2 and 11 LS/km^2 in coastal areas to the north and south of the city. Correlation with seismometer-based and monument overturning back-calculated ground motions suggests that a minimum peak ground acceleration (PGA) of approximately 0.2 g was necessary for landsliding throughout the region, but does not explain the subregional areas of high landslide concentration. However, analysis of topographic slope and the distribution of generally weak, dip-slope, geologic units does sufficiently explain why, on a sub-regional scale, high landslide concentrations occurred where they did. These include: (1) an inland region of steep, dip-slope, anticlinal sedimentary strata with associated fold belt compression and uplift of the anticline and (2) coastal areas with generally weaker, weathered outcrop lithology and steeper slopes resulting from active marine and terrestrial cliff processes. The results offer lessons for understanding the effects of earthquakes on both regional and subregional scales with regard to the spatial distribution of landsliding.

Published by Elsevier B.V.

1. Introduction

The July 16, 2007, M_w 6.6 Niigata Chuetsu–Oki earthquake occurred at 10:13 a.m. local time off the west coast of Honshu, Japan near the city of Kashiwazaki in southern Niigata Prefecture (Figure 1). The earthquake caused 11 fatalities, nearly 2000 injuries, about 1100 damaged residences (Kayen et al., 2009), and was responsible for the nearly two year closure of the Kashiwazaki–Kariwa power plant, the world's largest nuclear plant in terms of power production. In addition to extensive liquefaction and damage to roads, rail lines, bridges, port facilities, and structures, landslides occurred throughout the immediate onshore epicentral region (Figure 2). Damage from landslides was generally confined to transportation routes, and involved minor pavement cracking, roadway embankment failures, as well as complete destruction of road and railway sections. In only one known case was a residence damaged by a landslide; other infrastructure-related damage involved minor slope movements that caused small (<5 cm) deformations at the crest of several water-storage earth-embankment dams (Kayen et al., 2007). In general, reconnaissance data showed that the overall geographic pattern of most non-landsliding structural damage could be correlated with either the level of infrastructure design and construction or particular site-specific soil conditions (Kayen et al., 2007). However, we found the spatial distribution of observed landsliding to be heterogeneous and not easily explained by typical seismic source–distance metrics. Investigating and explaining these observations is the purpose of the study presented herein.

Landsliding is common from magnitude (M_w) 6+ earthquakes that affect steep terrain; extensive sliding was reported during all recent large earthquakes in mountainous areas of the United States (e.g., 1989 Loma Prieta, California — Keefer, 1998; 1994 Northridge,

* Corresponding author. Tel.: +1 650 329 5466.
E-mail addresses: bcollins@usgs.gov (B.D. Collins), rkayen@usgs.gov (R. Kayen), ytgeotec@tiger.kobe-u.ac.jp (Y. Tanaka).
[1] Tel.: +1 650 329 4195.
[2] Tel.:+81 78 803 6058.

0013-7952/$ – see front matter. Published by Elsevier B.V.
doi:10.1016/j.enggeo.2011.12.010

California — Harp and Jibson, 1996; 2002 Denali, Alaska — Jibson et al., 2004) and elsewhere (e.g., 1980 Irpinia, Italy — Wasowski et al., 2002; 2005 Kashmir, Pakistan — Harp and Crone, 2006; 2008 Wenchuan, China — Yin et al., 2009) including the 2004 M_w-6.6 mid-Niigata earthquake (e.g., Kyoji et al., 2005; Kieffer et al., 2006) located just 50 km inland from the event described here. These events provide direct empirical evidence for the spatial distribution of landsliding that can be expected from similar future earthquakes. Typically, correlations between landslide occurrence and seismological and spatial parameters are extracted from studies based on documented landslide inventories (e.g., Keefer, 1984, 2000; Harp and Wilson, 1995; Khazai and Sitar, 2004; Lee et al., 2008; Harp et al., 2011). These correlations can aid seismic landslide hazard analysis and planning for communities prone to earthquake-induced landsliding (e.g., Jibson et al., 2000; Parise and Jibson, 2000; Chang et al., 2006).

Spatial and seismological correlations offer one of the best predictors for expected landslide distributions resulting from earthquakes and are commonly based on magnitude–distance relationships, ground motions, and bedrock geology. Keefer (1984) presented a comprehensive set of correlations between landslide distance (e.g., as measured from the epicenter or fault plane) and earthquake magnitude; these correlations continue to be used for comparison with more recent (e.g., Rodríguez et al., 1999; Papadopoulos and Plessa, 2000) and regionally specific (e.g., Esposito et al., 2000; Wasowski et al., 2002) earthquake investigations. Additional work by Keefer (2000) showed that strong correlations also exist between the number of landslides and landslide distance — typically seismic shaking decreases at distance due to attenuation of energy within the subsurface. As a result, landslide concentration (the number of landslides per unit area) also generally decreases with increasing epicentral and fault-plane distance. In the 1989 Loma Prieta, California earthquake Keefer (2000) used power and exponential law functions to explain these effects. Harp and Wilson (1995) were the first to correlate instrumentally-recorded ground motions and landslide limits, and correlations based on measures of recorded peak ground acceleration (PGA) also exist for some additional earthquakes. However, these types of correlations are generally uncommon because many reconnaissance case histories lack a sufficiently dense collection of measurements over landslide-impacted areas. In one well-documented case, Khazai and Sitar (2004) showed that most landslides from the 1999 Chi-Chi, Taiwan earthquake occurred in areas with horizontal and vertical PGA levels of at least 0.15 *g* and 0.2 *g*, respectively. Finally, linkages to regional and site-specific geology have also led to improved understanding of earthquake-induced landslide distributions. Parise and Jibson (2000) for example, showed that a susceptibility index, defined by the ratio of area covered by landslide sources within a geologic unit to the total

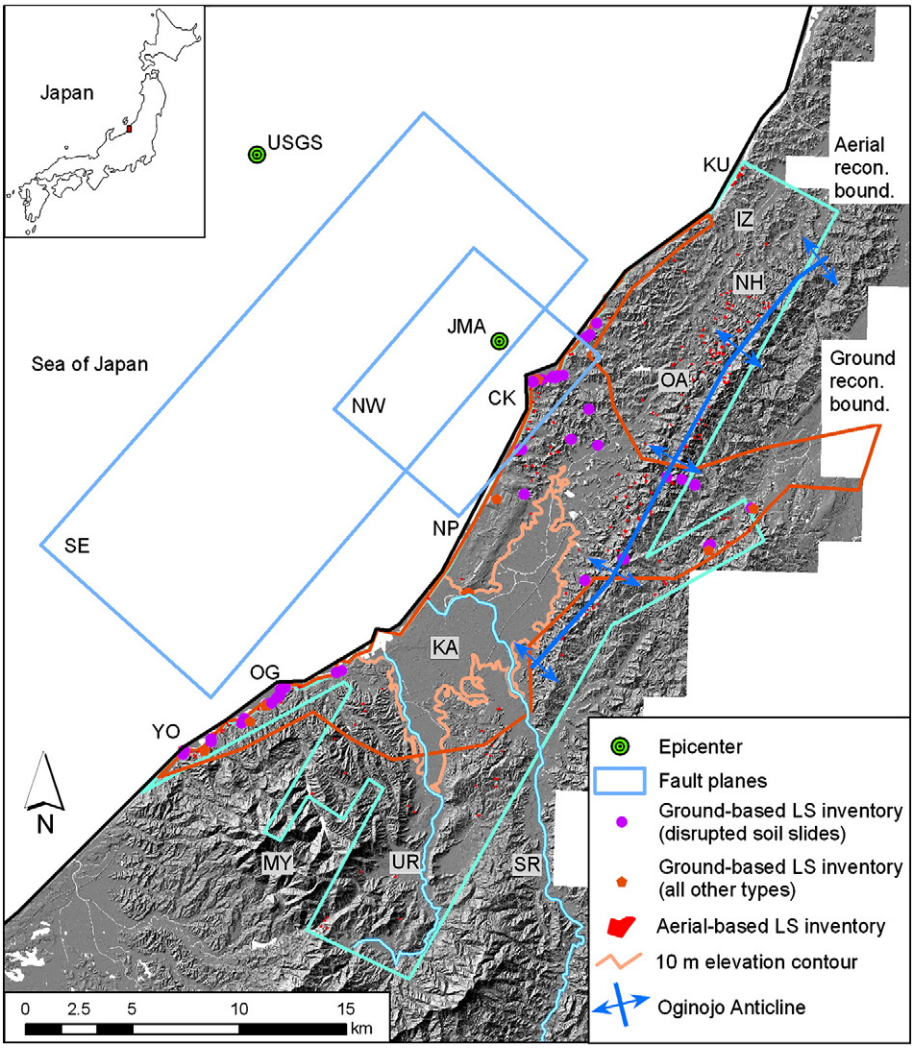

Fig. 1. Regional map of Kashiwazaki, Japan with 5 m DEM hillshade base showing USGS and JMA estimated epicenters, HERP (2008) based surface projections of dual and opposite dipping (SE and NW) fault plane ruptures, reconnaissance area boundaries, and landslides inventories. Place names referenced in the text are: KA: Kashiwazaki, NP: Kashiwazaki–Kariwa Nuclear Power Plant, SR: Sabaishi River, UR: U River, IZ: Izumozaki, NH: Nishiyama Hills, OA: Oginojo Anticline, KU: Kutsuta, CK: Cape Kannon, OG: Oumigawa, YO: Yoneyama, MY: Mt. Yoneyama.

Fig. 2. Coastal landslides (a) north of Kashiwazaki at 3 km JMA epicentral distance and (b) south of Kashiwazaki at 23 km JMA epicentral distance. Arrow in (a) identifies the location of the inset image.

outcrop area of each unit, could be used to distinguish areas of high versus low landslide susceptibility.

We investigated the 2007 Niigata Chuetsu–Oki earthquake to understand the spatial and seismological effects of an offshore earthquake on an urbanized and landslide-prone area (Kayen et al., 2009). During the investigation, we noted a heterogeneous and somewhat unexpected landslide distribution — especially with respect to the high density of mid-epicentral distance coastal landslides. Here, we present and use both new and existing landslide inventories from the earthquake, coupled with spatial and seismological analyses, to explore these high landslide concentration areas. Adapting existing methods, we examine the landslide distribution in terms of both regional and subregional settings, including analysis of topographic slope, bedrock geology and structure, and the offshore location of the earthquake epicenter and fault–rupture planes. Similar to previous studies (e.g., Wasowski et al., 2002) we postulate that significant characteristics of the expected landslide distribution can only be explained by investigating factors at both the regional and subregional scales.

2. Regional setting

Kashiwazaki is located on the Sea of Japan coast, about 300 km northwest of Tokyo. The Kashiwazaki region is characterized by steep, 10–50-m-tall coastal cliffs composed of Miocene, Pliocene and Pleistocene sedimentary units to the north, and Pliocene volcanic and sedimentary deposits to the south (Kobayashi et al., 1995). The coastal cliffs are bisected by a broad plain formed by the Sabaishi and U Rivers. The city of Kashiwazaki is located between these two rivers (Figure 1) on an extensive area of Holocene and Pleistocene sand-dune deposits. Farther inland, rugged hills several hundred meters in elevation, formed from Miocene sedimentary and volcanic units, have been compressed by a series of northeast-trending fold belts. Compressional tectonics have also produced many active thrust faults in the area, typically with north-northeast trend, both on- and offshore.

3. Seismological background

The Niigata Chuetsu–Oki earthquake was estimated at M_w 6.6 by the U.S. Geological Survey (USGS, 2007) based on teleseismic observations; these data indicated an epicenter located 24 km northwest of Kashiwazaki (Figure 1) set with a rupture focal depth of 10 km. Using local data, the Japanese Meteorological Agency (JMA, 2007) computed a similar magnitude (M_{JMA} 6.8) and focal depth (17 km) but with an epicenter located only 20 km northwest of Kashiwazaki and some 12 km east of the USGS-determined epicenter. Because the teleseismically-determined (USGS) epicenter is not located on the ruptured fault planes (see Figure 1), we used the locally-determined JMA epicenter for our analyses. All ensuing distance metrics are therefore based on the JMA epicenter (herein referred to simply as the epicenter).

The focal mechanism has been attributed to reverse-slip motion on a buried fault in an area of compressive deformation resulting from the collision of two smaller plates (Amur and Okhotsk) associated with Pacific–Eurasian plate subduction (USGS, 2007). NRI ESDP (2007) identified the two conjugate fault-plane solutions for the event as a

northwest (NW) dipping plane and a southeast (SE) dipping plane. Initial source inversions using strong-motion data alone were not able to distinguish which of the two focal planes ruptured (e.g. Aoi et al., 2007; Irikura et al., 2007; Koketsu et al., 2007; Takenaka et al., 2007; Toda, 2007). Additional work by Cirella et al. (2008), using both strong-motion and GPS data, also required the fault-plane dip direction to be inferred to explain the rupture process. However, using data collected with ocean-bottom seismometers along with a reevaluation of the strong-motion data, the Headquarters for Earthquake Research Promotion, HERP (2008) showed that rupture involved both planes; their explanation has rupture originating on the SE dipping plane with minor activation of the smaller NW dipping plane located to the northeast of the initiating rupture. This interpretation of aftershock data distinguishes a 27 km by 14 km, 40° SE dipping rupture plane with upper edge at 2 km depth, and a 10 km by 12 km, 50° NW dipping plane with upper edge at 4 km depth, both striking N40°E (Figure 1). We use these plane geometries for our landslide analyses.

4. Landslide inventories

We investigated landslides caused by the earthquake using a combination of ground-based field observations begun two days following the earthquake, oblique photo analysis, and subsequent analysis of third-party aerial-photo-based landslide inventories which utilized photos taken two days after the event. The inventories do not include landslides that could have occurred on Sado Island, located 30 km to the northwest, where only minor damage was reported.

We identified 70 landslides distributed over a 181 km^2 area (average landslide concentration, ALC = 0.4 LS/km^2) using ground-based reconnaissance observations from four teams of two persons distributed throughout the affected area (Kayen et al., 2007). This landslide total does not include minor roadbed slope failures, which were too numerous to accurately count. At each landslide, we recorded landslide type, material type, shear plane depth, and overall size. Care was taken to record only those landslides that were triggered by the earthquake as evidenced by fresh failure scarps or newly disturbed ground. For the ground-based inventory, we were generally able to confirm a seismic trigger, rather than a precipitation trigger, by observing either relatively dry soil conditions in landslide scarps or obvious new damage to infrastructure that could have only occurred as a result of the earthquake In some cases, we identified landslide type and estimated volume following the field work through analysis of oblique field photos and terrestrial LiDAR data collected during the original reconnaissance. Landslide types consisted of shallow (<3 m), disrupted soil slides (81%), deeper-seated soil slumps (14%), rock falls (3%), soil block slides (1%) and soil lateral spreads (1%), as classified according to Varnes' (1978) terminology. The low number of rock falls compared to that observed in other earthquakes (Keefer, 1984) is thought to be due to the lack of near-vertical rock outcrops in the region — most landslides failed by sliding rather than falling. Even on the relatively steep coastline, we observed mainly slide events. On the other hand, the high percentage of disrupted soil slides is consistent with that documented in other earthquakes (Keefer, 1984) including the nearby 2004 Niigata event (Kieffer et al., 2006). Landslide volumes were grouped into three categories: small (<100 m^2), medium (100–1000 m^3), and large (>1000 m^3). Most landslides (62%) were small owing to the large number of shallow, disrupted soil slides; there were approximately an equal number of medium (18%) and large (20%) landslides.

We used an aerial-photo-based landslide inventory provided by PASCO Corporation (PASCO) and Kokusai Kogyo Company Ltd. (Kokusai Kogyo, 2007) to corroborate our field inventory over a larger region. The PASCO–Kokusai Kogyo effort, performed immediately following the earthquake using GIS analysis of aerial photos taken on July 18 and 19, 2007, documented 312 landslides over a 332 km^2 area (ALC = 0.9 LS/km^2). Because of the emergency-response nature of the data collection mission, the data set was not able to be field checked at the time. Sato (2007), using the same aerial photos as those collected by PASCO–Kokusai Kogyo, later ground-truthed several of the larger landslides and recorded a slightly lower ALC (0.7 LS/km^2) in a smaller subset of the epicentral area, with 172 landslides identified over a 261 km^2 area. A first-order comparison of our ground-based inventory to the PASCO–Kokusai Kogyo data set does reveals several discrepancies between observed and mapped landslides, and we therefore believe that some of the landslides identified in the aerial photo reconnaissance may not have been seismically induced. Typhoon Man-yi passed along the Pacific coast of Japan just prior to the earthquake, and Niigata Prefecture pre-earthquake precipitation levels were above normal at that time (178% of average for the month of June; JMA, 2008) suggesting a precipitation-induced trigger for some aerial-photo-identified landslides. Yamagishi and Iwahashi (2007) documented more than 3000 landslides in this region following heavy precipitation in 2004, highlighting the high landslide susceptibility here to precipitation-induced landslides. However, Hasegawa et al. (2009) showed that high seismically-induced landslide concentrations (6.4 LS/km^2) from the 2007 event did occur in select areas of the affected region through field-checked aerial-photo analysis of landslides north of Kashiwazaki. Thus, despite the possibility of precipitation-induced landslides contaminating the aerial-based landslide inventory, we concluded that the data set is sufficiently robust and within acceptable bounds for performing statistical analysis.

5. Landslide distribution

Spatial distance metrics between landslides and earthquake sources provide a first order indication of the relative seismically-triggered landslide distribution throughout an affected region. Here, using a combination of GIS, CAD, and virtual-globe software packages, we analyze landslide concentration correlations with epicentral distance and with distance from the surface projection of the HERP (2008) defined fault planes. In these analyses, we use the entire surface projection of the fault planes (not just the updip edge) to account for the energy from the rupture of both planes.

Landslide concentration (LC), measured as the number of landslides divided by the area in which they occur for a set area boundary, describes the relative spatial distribution of landsliding throughout a region. In calculating LC, we ignored submarine areas because no observations were made in those locations. In addition, only those areas above a specific elevation threshold (in this case, 10 m) were included to focus the results on areas with steep, landslide-prone topography (e.g., similar to Keefer, 2000; Khazai and Sitar, 2004). In the Kashiwazaki region, the area located below 10 m elevation coincides with the primary flat, fluvial plain formed by the U and Sabaishi Rivers (Figure 1). Finally, we truncated the areas used for calculating landslide concentration at the respective aerial and ground-based reconnaissance boundaries, consistent with the approach used by Keefer (2000). This could have inflated LC values at the study area perimeter (due to the likelihood that there were few to no landslides outside this boundary, but still within the distance bin radius), however this is highly unlikely to significantly affect the results.

Our analyses of ground- and aerial-based landslide concentrations binned at 1-km increments for epicentral distance (Figure 3a) and distance from the fault plane surface projection (Figure 3b) show the expected quantitative decline in LC with increasing distance. These are consistent, in magnitude and trend, to other similar earthquakes with recorded landslide inventories (e.g., Keefer, 2000 — plotted as a smoothed trend line in Fig. 3 for the 1989 Loma Prieta, California earthquake; Khazai and Sitar, 2004 for the 1999 Chi-Chi, Taiwan earthquake). In addition, the maximum epicentral distance of a recorded landslide (29 km) is well within the expected boundaries for this magnitude event when compared to other historical earthquakes (Keefer, 1984). However, there are also considerable departures (i.e., here defined as generally those with greater than 1 LS/km^2 at either more than 10 km

epicentral distance or more than 2 km fault plane distance) from the relatively smooth decline with increasing distance. Although there is inherent variability in all such data sets due to the stochastic nature of landslide processes, these areas of high landslide concentration are also significantly larger than those found in similar magnitude earthquakes such as the 1989 Loma Prieta, California and 1999 Chi-Chi, Taiwan data sets (Keefer, 2000; Khazai and Sitar, 2004).

First order analysis indicates that landslide clusters coincide primarily with coastal areas. LC (using either ground- or aerial-based methods) is highest north of Kashiwazaki, near Cape Kannon and Kutsuta (7.9–10.9 LS/km^2 and 1.4 LS/km^2 at the 3 km and 14 km epicentral distance bins, respectively), and south of the city, between Oumigawa and Yoneyama (2.7–4.5 LS/km^2 at the 20–24 km epicentral distance bin). Only in the Nishiyama (West Mountain) Hills 10–12 km bin do concentrations coincide with something other than coastal landslides. Analysis of LC based on the distance from fault-plane surface projection (SE and NW rectangles in Figure 1) shows similar trends (Figure 3b). Landslide concentration is highest (2.8–4.8 LS/km^2, 1.5 LS/km^2, and 1.4 LS/km^2) near the coast (0–0.5 km, 2–3 km, and 8 km fault plane distance bins respectively) and in the inland Nishiyama Hills (LC up to 2.2 LS/km^2 at the 5–7 km bin fault plane distance).

These concentrations are significant in that they potentially represent areas of increased landslide hazard from earthquakes that affect coastal regions. However the reason for their occurrence in not necessarily obvious. They may represent either a spatial non-uniformity in landslide-susceptible slopes (i.e., due to steeper slopes or poor geologic conditions) or differential seismic attenuation, and possibly amplification, within the region. We therefore examine the concentrations in this context to deduce which of the two is the more plausible explanation.

6. Correlation with ground motion

Differential attenuation and amplification of seismic ground motion at a regional scale offers a potential explanation for the high landslide concentration areas identified in the landslide inventories. Various measures of ground motion and related intensity forms, including

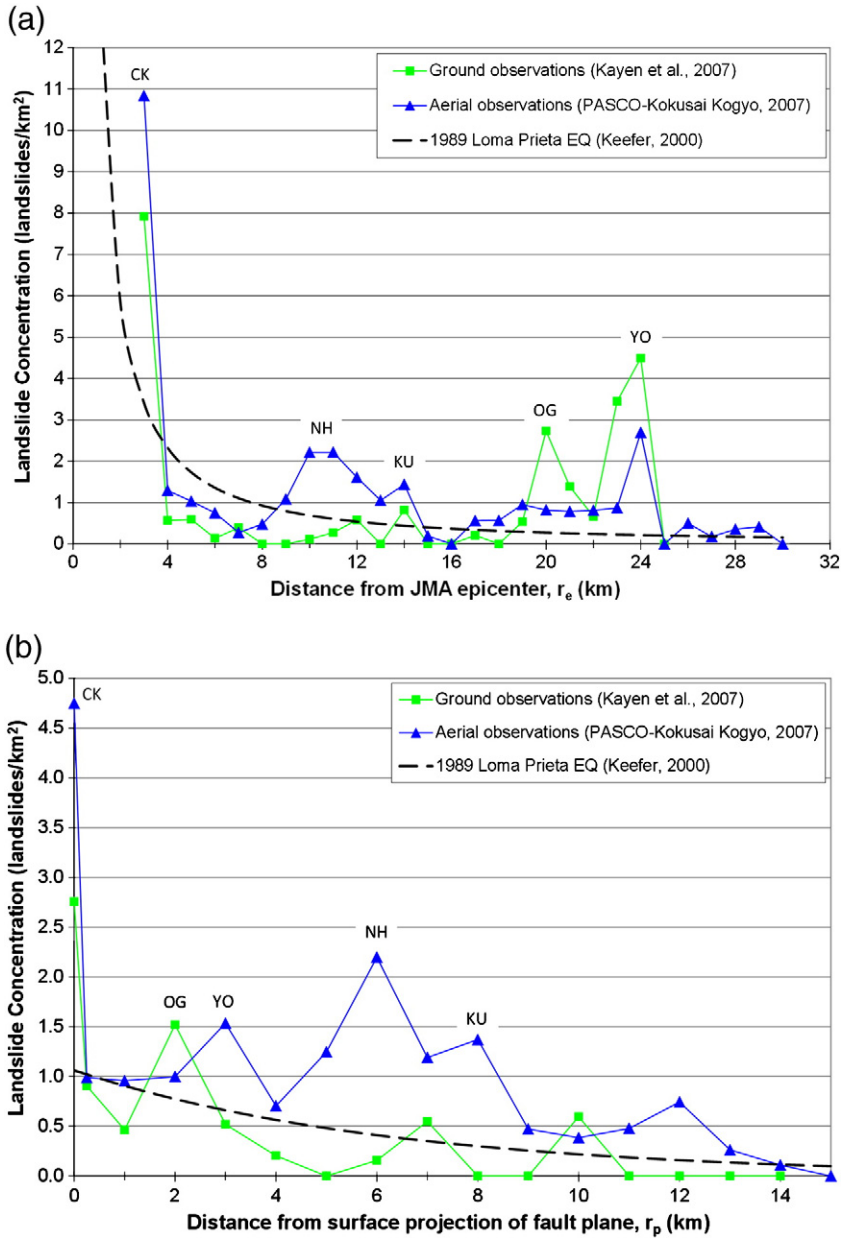

Fig. 3. Landslide concentration as a function of (a) JMA epicentral distance and (b) surface projection of fault plane distance. Data from Keefer (2000) on the 1989 Loma Prieta, California shown for comparison. Labels coincide with place names in Fig. 1.

Modified Mercalli Intensity (Keefer, 1984), Arias Intensity (Wilson and Keefer, 1985; Harp and Wilson, 1995; Lee et al., 2008), and peak ground acceleration (Khazai and Sitar, 2004; Wang et al., 2010) have been proposed and used for spatial correlation of landslides. Arias Intensity has a strong correlation with the distribution of earthquake-induced landslides, but it can only be derived from instrumental records. In Kashiwazaki, only a few stations were near the landslide-affected areas. We therefore selected horizontal PGA (herein referred simply as PGA) to measure the influence of ground motion on landslide distribution. PGA is useful in that it directly accounts for particularities of fault rupture such as directivity and hanging-wall effects. Southwestward (towards Kashiwazaki) directivity pulses were noted in source inversion studies (e.g. Cirella et al., 2008; Takenaka et al., 2009; Miyake et al., 2010) and all landslides in this event were located on the hanging wall of the main SE rupture plane (Figure 1). Thus, the use of PGA here eliminates the need to consider these effects separately with respect to landslide triggering.

Our PGA measurements used for correlation come from three sources: motions from the seven nearest recordings (NIG seismometer stations, K-NET, 2008; Table 1), motions recorded from the combined EW–NS components at the Kashiwazaki–Kariwa Nuclear Power Plant (KKNPP) foundation mat (TEPCO, 2008; Table 1), and motions back-calculated from monument overturning observations. Observations of overturned cemetery and shrine monuments (Figure 4; Kayen et al., 2007; Tobita et al., 2007; Yamagishi et al., 2007) provide an indication of ground motions. Monument topples during earthquakes are common in Japan (e.g., Ikegami and Kishinouye, 1950; Omote et al., 1977) due to the design of many shrine tombstones that do not key in to underlying support stones.

A simple calculation using West's formula (Milne, 1885) comparing the seismic (a_c) and restoring (gravitational acceleration, g) moments needed to initiate uplift, rocking, and subsequent toppling of a block around one edge is possible if the geometry (relative width, b to height, h ratio, b/h) of the toppled block is known:

$$a_c > \frac{b}{h} g \tag{1}$$

This analysis requires that the monument basal friction was sufficient to prevent sliding — a point supported by our field observations. Others have performed similar calculations (e.g., Housner, 1963; Yim et al., 1980; Ishiyama, 1982; Winkler et al., 1995), and despite recent debate on the applicability of the method for determining complex earthquake motions (e.g. Apostolou et al., 2007), the method is still applicable for determining a lower bound for monument rocking ground motions (i.e., PGA may be higher to initiate toppling).

We used observations from thirteen sites with overturned monuments, located between 4 and 17 km epicentral distance, to calculate b/h ratios, and therefore equivalent minimum PGA values (by Eq. (1)) ranging between 0.17 g and 0.5 g (Table 1). Only the most slender blocks, and thereby most prone to toppling, were used to provide a conservative basis for ground response. Even with these restrictions, topple ratios (number of monuments toppled to total number of monuments) averaged nearly 70% and were 100% at many sites indicating that minimum shaking levels for toppling were ubiquitous at these sites. These results provide reasonable estimates for ground motion in areas where recorded measurements do not exist, although it is important to note that the true "peak" ground acceleration may have been higher than that calculated from this "minimum peak" analysis.

The computed PGA contours (Figure 5) from statistical kriging of all PGA data indicate a minimum threshold for landsliding of approximately 0.18 g. This is consistent with previous research; Khazai and Sitar (2004) found a similar horizontal PGA threshold (0.15 g) for landsliding in the 1999 M_w7.3 Chi-Chi, Taiwan earthquake as did Wang et al. (2010) in a regional analysis from the 2008 Wenchuan, China earthquake. PGA was highest in the central Kashiwazaki coast area (as shown by the seismometer-based measurements that define two bulls-eye contours there) but caused few landslides in the flat topography of this region. In areas with high landslide concentration such as the Nishiyama Hills and coastal areas north and south of Kashiwazaki, PGA values range from 0.2 g to 0.35 g and no increased correlation between PGA and landslide distribution is apparent. Due to a lack of PGA measurements in the main landslide-affected areas, it is possible that accelerations were higher, for example, as a result of topographic amplification not exhibited in other PGA measurements and estimates. Given that the ratio of topographic

Table 1
Seismometer data and estimated ground motions from back-calculation of monument topples.

Site number[a]	Site description	JMA epicentral distance (km)	Recorded or back-calculated horizontal PGA[b] (g)
NIG016	K-NET seismometer station	22	0.43
NIG017	K-NET seismometer station	22	0.32
NIG018	K-NET seismometer station	14	0.86[c]
NIG019	K-NET seismometer station	29	0.60
NIG021	K-NET seismometer station	43	0.35
NIG024	K-NET seismometer station	44	0.25
NIG025	K-NET seismometer station	50	0.29
KKNPP	Foundation mat seismometer	8	0.76
BC-TT1	Cemetery	4	0.33
RK14	Konsengi Temple	12	0.39
RK29	Shrine/cemetery	6	0.29
RK42	Shrine	10	0.18
RK43	Cemetery	10	0.35
RK44	Cemetery	10	0.37
RK48	Cemetery	14	0.31
RK54	Cemetery	11	0.39
RK58	Tombstone monument store	15	0.18
SA13	Rock wall	16	0.50
SD04	Shrine	17	0.17
SD16	Temple	13	0.50
SP40	Monument	14	0.31

[a] Site numbers are referenced to Kayen et al. (2007).
[b] Back-calculated values indicate minimum PGA. Values could be higher in all cases.
[c] Kayen et al. (2007) indicates potential liquefaction at this site and Cirella et al. (2008) showed difficulty with matching observed PGA to modeled source inversions. PGA may therefore have been higher.

Fig. 4. Toppled monuments at 12 km JMA epicentral distance with approximate 90% topple ratio. Typical width and height of the most slender blocks (arrow) is 25 cm by 75 cm ($b/h = 0.33$).

relief at the coast (H; 30 to 80 m) to the incident seismic-wave length (λ; 30 to 100 m; Kayen et al., 2007; K-NET, 2008) is near unity ($H/\lambda = 0.2$ to 2.7) suggests that topographic amplification of the steep cliffs may have occurred, potentially increasing PGA by 25 to 50% (e.g., Ashford et al., 1997; Harp and Jibson, 2002). However, the incident angle of incoming seismic waves (~40° as calculated from the major southeast dipping fault plane; HERP, 2008) toward the coastal slopes was less likely to have induced topographic amplification because the coastal slopes are aligned facing, rather than away from the seismic source. In such cases, deamplification of PGA commonly occurs (e.g., Ashford and Sitar, 1997; Meunier et al., 2008). We therefore judge that topographic amplification did not take place and does not offer an explanation for high PGA levels or increased landslide concentrations near the coast.

7. Correlation with geologic and topographic conditions

The lack of explanation offered by ground motion response for high landslide concentrations in both coastal and inland areas dictates that susceptibility characteristics such as slope inclination and geological substrate be investigated. This includes analysis at both the regional (Kashiwazaki-wide) and sub-regional (coastal, inland areas) scales.

7.1. Correlation with topographic slope

We investigated the correlation between topographic slope and landsliding through GIS analysis of a 5 m DEM available for the majority of the Kashiwazaki region (Figure 1). Using only the data within each of the ground and aerial reconnaissance boundaries, all DEM-generated slope cells were binned in 5° increments (Figure 6a). Mean (14°, 18°) and maximum (85°, 85°) values for the ground and aerial reconnaissance areas, respectively, are consistent and highlight the varying topography of the region. Using the same slope map, we determined the maximum slope angle of each landslide for both ground and aerial inventories (Figure 6b). These results indicate that the majority of landslides were triggered on relatively steep slopes averaging 42° and 45° for the aerial and ground-based inventories, respectively.

Normalizing each landslide maximum slope angle bin for contributing slope angle area (i.e., deriving a slope-angle-based landslide concentration by dividing Figure 6b by Figure 6a) highlights this observation, namely, that steep slopes failed ubiquitously with normalized landslide concentrations exceeding 900 LS/km^2 within the steepest slopes (Figure 7). The highest, seemingly unreasonable, landslide concentration values are a product of the low frequency of occurrence of steep slopes (Figure 6a) in the region coupled with the high frequency of occurrence of landslides on those slopes. Similar to previous studies (e.g., Keefer, 2000) the overall relationship is exponential and the data is well fit by trend lines for both ground and aerial-based inventories. Interestingly, the point of maximum exponential curvature (~45°, defined as $\kappa = f''(x)/(1+f'(x)^2)^{3/2}$, where $f(x)$ is the exponential function in Fig. 7, and not entirely obvious when plotted in linear space) is approximately 10° greater than that found in other studies (Keefer, 2000 — 34°; Wasowski et al., 2002 — 35°). We interpret this as a further indication that the steepest slopes were particularly susceptible to landsliding during this earthquake.

The areas of high landslide incidence (coastal areas and Nishiyama Hills) can be investigated in more detail by calculating the average of the maximum slope angles for all landslides contained in each subregion. The results (Table 2) are generally consistent between the ground and aerial-based inventories, and indicate that coastal landslides occurred in areas with very steep (40° to 65°) slopes. In all subregions, average values are on the order of the point of maximum curvature (45°) previously identified indicating that these areas are in the particularly susceptible range for landsliding based on slope. Despite this seemingly strong correlation between slope and areas of high landslide concentration, there are other areas within the region that have slopes equal to or exceeding the landslide values which did not experience significant landsliding. For example, in the vicinity of Mount Yoneyama, (Figure 1) at the southern end of the study region, slopes are significantly steep (>50°) but had few documented landslides. Thus, whereas slope alone explains much of the landslide distribution, it does not entirely explain the high landslide concentration areas.

7.2. Correlation with geology

We performed additional GIS analysis to investigate potential correlations between bedrock geologic unit and the landslide

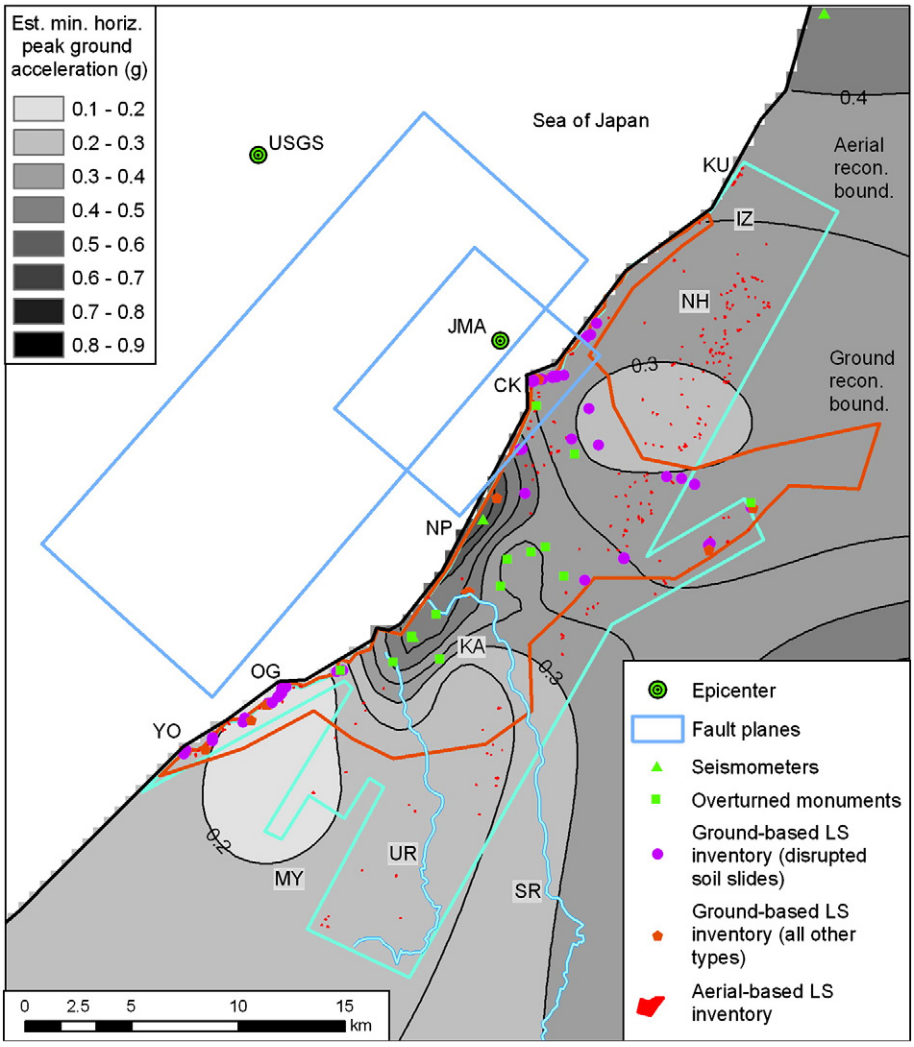

Fig. 5. Estimated minimum peak horizontal ground acceleration contour map from seismometer and overturning monument data (see Table 1). Some seismometer measurements are outside the region shown and incorporate site effects at those locations. Place names denoted by initials (i.e., "CK") are described in Fig. 1.

inventories. Using existing geological mapping of the Kashiwazaki region (Kobayashi et al., 1989, 1993, 1995, and Takeuchi et al., 1996), we simplified the overall geology into eight units (Figure 8) and calculated geology-normalized landslide concentrations for each landslide inventory. The results (Figure 9) indicate that several units were particularly susceptible to landsliding, namely Pliocene and Miocene sedimentary units, typically consisting of sandstones and mudstones, and interestingly, Pleistocene dune sands. The sand dunes are part of the Arahama sand dune complex and, in the lower (Pleistocene) beds, are bonded by weak clay-organic cementation (Tazaki et al., 1989). Although the outcrop area of the Pleistocene beds is relatively small in the Kashiwazaki region (~2 km^2), weakly cemented sands are particularly susceptible to failure from seismic shaking (Sitar and Clough, 1983).

Compared to the M6.7 Northridge, California, USA earthquake in which geology-normalized landslide concentrations were also calculated (Parise and Jibson, 2000), our landslide concentration results are generally "low" (<3 LS/km^2). However, in the Northridge event, the number of landslides (~11,000) was much higher. Our estimates are comparable to those calculated from the 1980 Irpinia, Italy earthquake (Wasowski et al., 2002) in which values were generally less than 1 LS/km^2 and in which there were fewer landslides (~200). Overall, we were not able to distinguish particularly susceptible areas of our landslide distribution based on geology alone. For example, whereas the high landslide concentration in the Nishiyama Hills was generally located within Pleistocene sedimentary units (Figure 8), these units outcrop over a wide area of the region where landslides did not occur. We must therefore turn to subregional analyses of the high landslide concentration areas to explain the observed landslide distribution from the earthquake.

8. Analysis of high landslide concentration areas

8.1. Nishiyama Hills landslide concentration

The Nishiyama Hills, located south of Izumozaki, showed a high landslide concentration from the aerial reconnaissance data (the ground-based effort did not completely investigate this area). Our ground-motion correlations indicate a negative correlation with PGA; here, values decreased as the landslide concentration increased. However, as shown by our analyses, topographic slope and geology did correlate, in part with the high incidence of landsliding here. Namely, steep (>40°) Miocene and Pleistocene sedimentary slopes can be identified as the source for most of the documented landsliding. In contrast, the similarly steep slopes in the Mount Yoneyama area and which did not experience widespread landsliding are composed of mid-Pliocene volcanic units. On the subregional scale, the localized geologic structure of the Nishiyama Hills also likely influenced the increased susceptibility to landsliding. Here, the late-Cenozoic, Oginojo anticline with steeply (60° to 90°) dipping sedimentary limbs extends

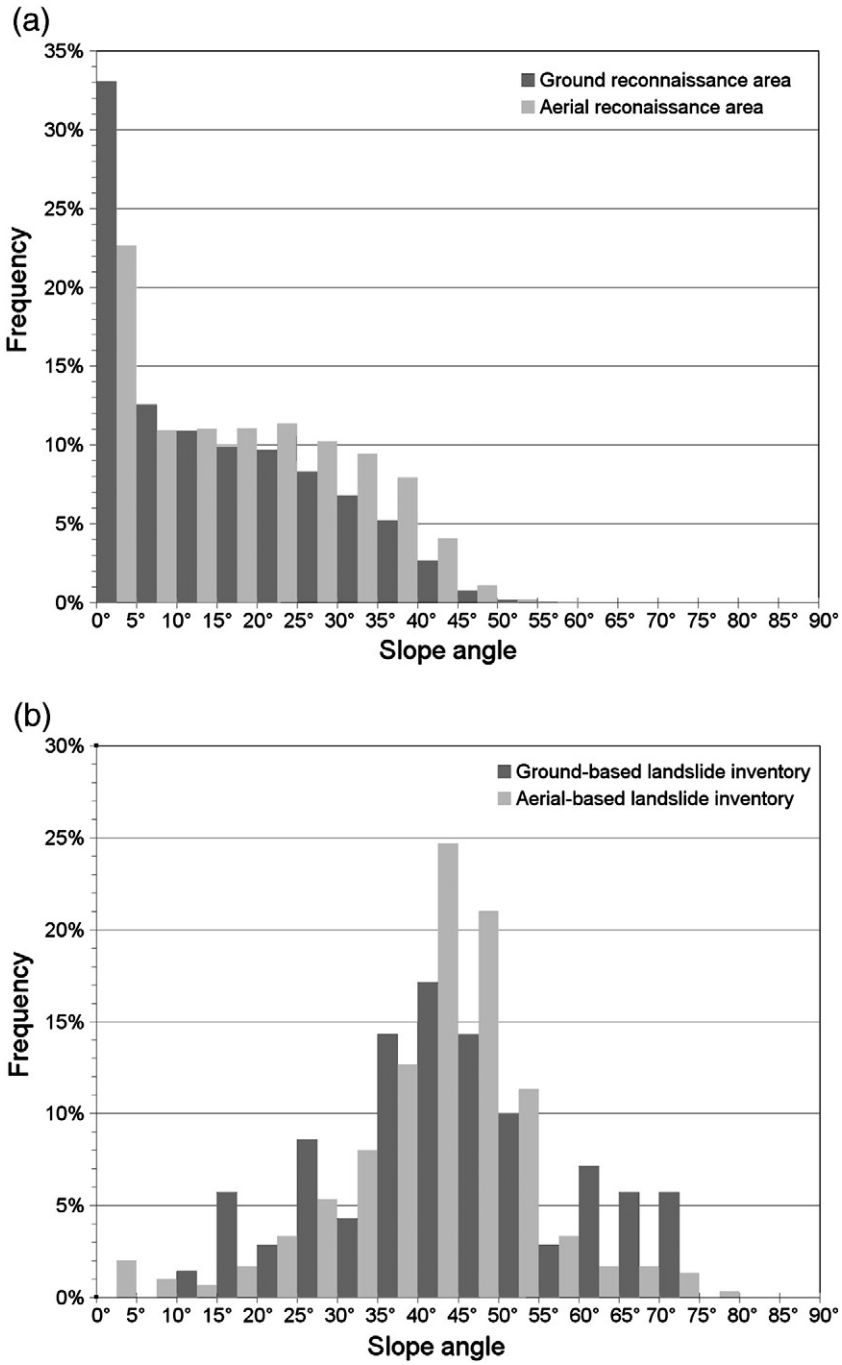

Fig. 6. Slope angle frequency distribution for (a) all slopes within each reconnaissance boundary, and (b) maximum slope angle for each landslide inventory.

from northeast to southwest along the length of the high landslide concentration zone (Figure 8, Kobayashi et al., 1993; Kobayashi et al., 1995). We suggest that this structure provided ample opportunity for dip-slope failures on subvertical, alternating mudstone and sandstone sequences. Although this line of reasoning can explain the elevated landslide concentration in the Nishiyama Hills, we suggest one other possible explanation. Nishimura et al. (2008) noted aseismic, compression and uplift of up to 4 cm to the west of and along the Oginojo anticline following the earthquake, indicating that the fold–belt itself underwent additional deformation separate from the thrust movement of the 2007 offshore fault rupture. Synthetic aperture radar (SAR) studies also noted uplift here with up to 10 cm measured over a 15 km long by 1.5 km wide area on the west side of the Nishiyama Hills (HERP, 2008). The results from Nishimura et al. (2008) suggest that this deformation is a result of a static stress increase in either the northwest dipping fault plane (Figure 1) or another weak shallow fault running beneath the anticline. In either scenario, the stress increase could have caused slope-weakening strain increases in the near surface (e.g., Morton et al., 1989), thereby also leading to an increase in landslide susceptibility in this region.

8.2. Coastal area landslide concentrations

A combination of steep slopes and weak geologic unit strength also likely caused the above-average landsliding along the coast during the earthquake. Whereas ground motions were not high in all areas of the coast, steep slopes formed in geologic units with high susceptibility are ubiquitous here. The slope correlation data show that the four

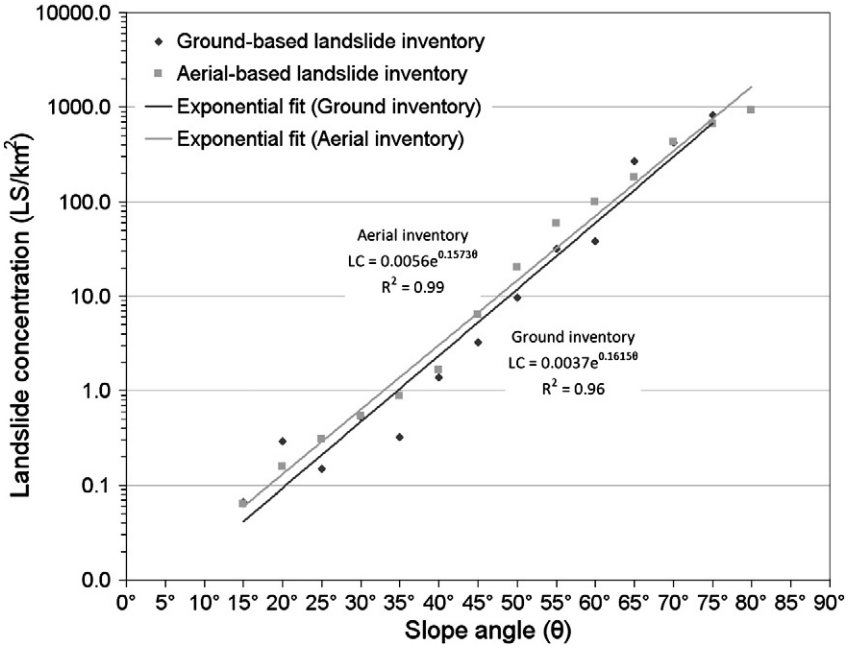

Fig. 7. Slope-normalized landslide concentration and exponential trend lines for landslide inventory data between 15° and 80°. The highest values are a result of the low frequency of occurrence of the steepest slopes.

coastal areas with high landslide concentrations (Kutsuta, Cape Kannon, Oumigawa, and Yoneyama; Figure 3) all have higher than average slopes for the region (Table 2, Figure 6) insinuating that the coastline was particularly susceptible to seismic shaking. Although this observation is not new for cliffed coastlines (e.g., Griggs and Scholar, 1997) our analyses provide quantitative data to bracket the degree of susceptibility (Figure 7). The coastal landslide areas also generally corroborate positively with the weaker geologic units of the area, in particular Pleistocene, Pliocene, and Miocene sedimentary units. Although the general correlation between geology and landsliding is not strong (Figure 9), field observations (Kayen et al., 2007) and laboratory testing by Gratchev and Towhata (2008) at the site of the Oumigawa landslide (OG — Figure 1; Figure 10) indicate that surficial materials along the coast are particularly weak, especially in cyclic shaking. Finally, we posit that the weathered, weakened state of bedrock from coastal influence may also have been a causative factor for the increase in observed landsliding in these areas. Under constant wave action, groundwater seepage, and cliff-face erosion, many coastal slopes are likely in a metastable state that requires very little seismic ground motion to fail. Our field observations indicate pre-failure coastal landslide slopes had inclinations upwards of 40° in many cases and earthquake-induced slide planes generally occurred in highly weathered, landslide-prone materials (Kayen et al., 2007). This enhanced susceptibility suggests that, in a geomorphologic sense, earthquake-induced coastal landslides could be identified separately from inland landslides when determining spatial correlations (i.e. plotting a coastal landslide threshold curve above that determined for all landslides from Keefer, 2000, for example; see Figure 3). Whereas the Niigata Chuetsu–Oki earthquake provides such an example, to date, there are insufficient processed case studies to develop such an approach.

Table 2
Subregional landslide inventory slope statistics.

Subregion	Ground-based landslide inventory average[a]	Aerial-based landslide inventory average[a]
Kutsuta (KU)	n/a[b]	43°
Cape Kannon (CK)	41°	39°
Oumigawa (OG)	63°	56°
Yoneyama (YO)	52°	53°
Nishiyama Hills (NH)	n/a	42°

[a] Averages denote the mean of the maximum DEM grid cell values in proximity to each landslide.
[b] n/a denotes detailed data not available for this region.

9. Conclusions

The 2007 M_w 6.6 Niigata Chuetsu Oki earthquake caused extensive landsliding throughout the Kashiwazaki area of Japan. Whereas the average landslide concentration from this event (0.4–0.9 LS/km^2) is low compared to the nearby 2004 Niigata Chuetsu, Japan earthquake (up to 30 LS/km; Kieffer et al., 2006), it is similar to other recent earthquakes having slightly greater magnitudes (0.5 LS/km^2 in the 1989 M_w 6.9 Loma Prieta, California — Keefer, 2000; ~1.1 LS/km^2 in the 1994 M_w 6.7 Northridge, California — Harp and Jibson, 1996). Compared to the 2004 Niigata earthquake, the 2007 event affected an area of lower topographic relief and without as great a known landslide hazard. The 2007 earthquake also occurred during drier conditions compared to the 2004 earthquake (i.e., in 2004, ten typhoons occurred in Japan before the earthquake; Kieffer et al., 2006), and was epicentered farther from susceptible slopes, thus explaining the lower landslide concentration in 2007.

In addition to documenting the major landslide effects of the earthquake, our analysis of existing aerial and ground-based landslide inventories identified two areas of particularly high landslide concentration that are not easily explained by typical measures of seismic correlation (i.e., seismic source distance and PGA). Susceptibility factors related to steep slopes and weak geologic units appear to have caused the occurrence of these high landslide concentrations. In the Nishiyama Hills, steep dip-slopes in potentially weak sedimentary strata coupled with aseismic uplift and compression of an anticline fold belt were likely responsible for increased landsliding. In the coastal areas, steep, weakened slopes under the influence of wave erosion and groundwater seepage were particularly susceptible to slope failure, suggesting that coastal slopes, in general, may be more susceptible to earthquake-induced failure. Whereas the presented results explain the landslide distribution from only one earthquake, they highlight the need for both regional and subregional ground motion and susceptibility

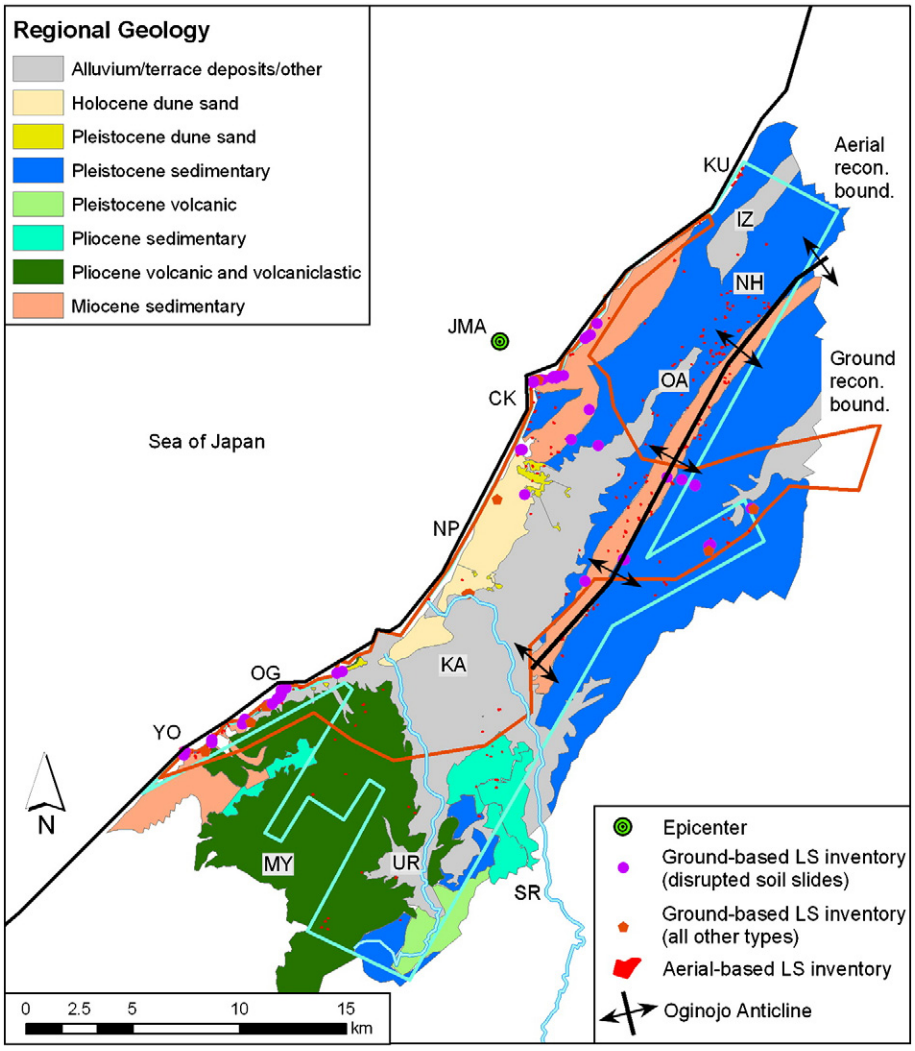

Fig. 8. Simplified geological map of the Kashiwazaki region (adapted from Kobayashi et al., 1989, 1993, 1995, and Takeuchi et al., 1996). Place names denoted by initials (i.e., "CK") are described in Fig. 1.

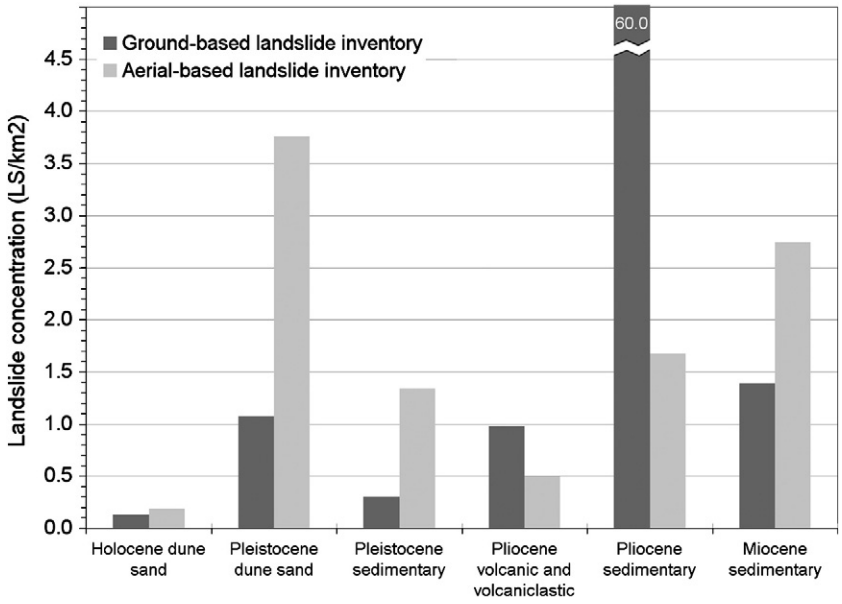

Fig. 9. Geology-normalized landslide concentration for landslide inventory data within select geological units. Data for alluvium and Pleistocene volcanics are not shown due to their low landslide concentration. High value for ground-based landslide inventory data in Pliocene sedimentary units is due to a single small outcrop located between Oumigawa (OG) and Yoneyama (YO) in the ground-based reconnaissance area (see Figure 8).

Fig. 10. The Oumigawa train station landslide located south of Kashiwazaki exemplifies the metastability and high seismic susceptibility that many coastal slopes exhibited.

analysis in explaining potentially complex documented landslide distributions from earthquakes.

Acknowledgments

Funding for the field component of this work was provided by the Geo-Engineering Earthquake Reconnaissance (GEER) and Earthquake Engineering Research Institute (EERI) activities of the U.S. National Science Foundation (Grants CMMI-0323914 and CMMI-0131895), and cost sharing by the U.S. Geological Survey. We acknowledge the use of aerial-based landslide datasets collected, processed and provided by PASCO Corporation and Kokusai Kogyo Company Ltd of Japan and thank Yoko Tamura (PASCO) for assistance with obtaining the datasets. Mark Reid (USGS), Randall Jibson (USGS), and two anonymous reviewers provided helpful reviews that increased the quality of this manuscript.

References

Aoi, S., Sekiguchi, H., Morikawa, N., Ozawa, T., Kunugi, T., Shirasaka, M., 2007. Source process of the 2007 Niigata-ken Chuetsu–oki earthquake derived from near-fault strong motion data. Eos Transactions AGU 88 (52), S54A-04 Suppl. Abstract.

Apostolou, M., Gazetas, G., Garini, E., 2007. Seismic response of slender rigid structures with foundation uplifting. Soil Dynamics and Earthquake Engineering 27, 642–654.

Ashford, S.A., Sitar, N., 1997. Analysis of topographic amplification of inclined shear waves in a steep coastal bluff. Bulletin of the Seismological Society of America 87 (3), 692–700.

Ashford, S.A., Sitar, N., Lysmer, J., Deng, N., 1997. Topographic effects on the seismic response of steep slopes. Bulletin of the Seismological Society of America 87 (3), 701–709.

Chang, K.-T., Chiang, S.-H., Hsu, M.-L., 2006. Modeling typhoon- and earthquake-induced landslides in a mountainous watershed using logistic regression. Geomorphology, vol. 89(3–4). Elsevier, pp. 335–347.

Cirella, A., Piatanesi, A., Tinti, E., Cocco, M., 2008. Rupture process of the 2007 Niigata-ken Chuetsu–oki earthquake by nonlinear joint inversion of strong motion and GPS data. Geophysical Research Letters 35, L16306. doi:10.1029/2008GL034756.

Esposito, E., Porfido, S., Simonelli, A.L., Mastrolorenzo, G., Iaccarino, G., 2000. Landslides and other surface effects induced by the 1997 Umbria–Marche seismic sequence. Engineering Geology 58, 353–376.

Gratchev, I., Towhata, I., 2008. Analysis of a slope failure triggered by the 2007 Chuetsu Oki Earthquake. Proceedings of the Int. Consortium on Landslides, 1st World Landslide Forum, Tokyo Japan, November 2008, pp. 396–399.

Griggs, G.B., Scholar, D.C., 1997. Coastal erosion caused by earthquake-induced slope failure. Shore and Beach 64 (4), 2–8.

Harp, E.L., Crone, A.J., 2006. . 13 pp. Landslides triggered by the October 8, 2005, Pakistan earthquake and associated landslide-dammed reservoirs: *U.S. Geological Survey Open-file Report 2006–1052* http://pubs.usgs.gov/of/2006/1052/. available on the World Wide Web at URL.

Harp, E.L., Jibson, R., 1996. Landslides triggered by the 1994 Northridge, California, earthquake. Bulletin of the Seismological Society of America 86 (1B), S319–S332.

Harp, E.L., Jibson, R., 2002. Anomalous concentrations of seismically triggered rock falls in Pacoima Canyon: are they caused by highly susceptible slopes or local amplification of seismic shaking? Bulletin of the Seismological Society of America 92 (8), 3180–3189.

Harp, E.L., Wilson, R.C., 1995. Shaking intensity thresholds for rock falls and slides: evidence from the 1987 Whittier Narrows and Superstition Hills earthquake strong motion records. Bulletin of the Seismological Society of America 85 (6), 1739–1757.

Harp, E.L., Keefer, D.K., Sato, H.P., Yagi, H., 2011. Landslide inventories: the essential part of seismic landslide hazard analyses. Engineering Geology 122 (1–2), 9–21.

Hasegawa, S., Dahal, R.K., Nishimura, T., Nonomura, A., Yamanaka, M., 2009. DEM-based analysis of earthquake-induced shallow landslide susceptibility. Geotechnical and Geological Engineering 27, 419–430.

HERP, 2008. The Niigata-ken Chuetsu–oki Earthquake in 2007: fault plane evaluation. Earthquake Research Committee of the Headquarters for Earthquake Research Promotion, Report dated January 11, 2008. http://www.jishin.go.jp/main/chousa/08jan_chuetsu_oki/p06-e.htm. Accessed 2 March 2010.

Housner, G.W., 1963. The behavior of inverted pendulum structures during earthquakes. Bulletin of the Seismological Society of America 53 (2), 403–417.

Ikegami, R., Kishinouye, F., 1950. The acceleration of earthquake motion deduced from overturning of the gravestones in case of Imaichi earthquake on Dec. 26, 1949. Bull. Earthquake Research Institute, Tokyo Univ, vol. 28, pp. 121–128.

Irikura, K., Kagawa, R., Miyahoshi, K., Kurahasi, S., 2007. Rupture process and strong ground motions of the 2007 Niigata-ken Chuetsu–Oki earthquake — directivity pulses striking the Kashiwazaki–Kariwa Nuclear Power Plant. Eos Transactions AGU 88 (52), S31B-0441 Suppl., Abstract.

Ishiyama, Y., 1982. Motions of rigid bodies and criteria for overturning by earthquake excitations. Earthquake Engineering and Structural Dynamics 10, 635–650.

Jibson, R.W., Harp, E.L., Michael, J.A., 2000. A method for producing digital probabilistic seismic landslide hazard maps. Engineering Geology 58, 271–289.

Jibson, R., Harp, E., Schulz, W., Keefer, D., 2004. Landslides triggered by the 2002 Denali fault, Alaska, earthquake and the inferred nature of the strong shaking: Denali Fault, Alaska, earthquake. Earthquake Spectra 20 (3), 669–691.

JMA, 2007. Japan Meteorological Agency: On the earthquake which occurred off Jo–Chuetsu in Niigata Prefecture around 10:13 on July 16, 2007. http://www.jma.go.jp/jma/press/0707/16a/kaisetsu20070716.pdf. (in Japanese), Accessed 1 July 2009.

JMA, 2008. Japan Meteorological Agency, Monthly Climate Reports for Niigata, Station No. 47604. http://www.data.jma.go.jp/obd/stats/data/en/smp/index.html. Accessed 1 May 2008.

Kayen, R., Collins, B.D., Abrahamson, N., Ashford, S., Brandenberg, S.J., Cluff, L., Dickenson, S., Johnson, L., Kabeyasawa, T., Kawamata, Y., Koumoto, H., Marubashi, N., Pujol, S., Steele, C., Sun, J., Tanaka, Y., Tokimatsu, K., Tsai, B., Yanev, P., Yashinsky, M., Yousok, K., 2007. . 230 pp Investigation of the M6.6 Niigata–Chuetsu Oki, Japan, Earthquake of July 16, 2007: *U.S. Geological Survey, Open File Report 2007–1365.* http://pubs.usgs.gov/of/2007/1365/. available on the World Wide Web at URL.

Kayen, R., Brandenberg, S.J., Collins, B.D., Dickenson, S., Ashford, S., Kawamata, Y., Tanaka, Y., Koumoto, H., Abrahamson, N., Cluff, L., Tokimatsu, K., 2009. Geoengineering and seismological aspects of the Niigata–Chuetsu Oki earthquake of 16 July 2007. Earthquake Spectra 25 (4), 777–802.

Keefer, D.K., 1984. Landslides caused by earthquakes. Geological Society of America Bulletin 95, 406–421.

Keefer, D.K. (Ed.), 1998. The Loma Prieta, California, earthquake of October 17, 1989 — landslides. U.S. Geological Survey Prof. Paper 1551-C. 185 pp.

Keefer, D.K., 2000. Statistical analysis of an earthquake-induced landslide distribution — the 1989 Loma Prieta, California event. Engineering Geology 58, 231–249.
Khazai, B., Sitar, N., 2004. Evaluation of factors controlling earthquake-induced landslides caused by the Chi-Chi earthquake and comparison with the Northridge and Loma Prieta events. Engineering Geology 71, 79–95.
Kieffer, D.S., Jibson, R., Rathje, E.M., Kelson, D., 2006. Landslides Triggered by the 2004 Niigata Ken Chuetsu, Japan, Earthquake. Earthquake Spectra 22 (S1), S47–S73.
K-NET, 2008. Kyoshin Network of the National Research Institute for Earth Science and Disaster Prevention. http://www.k-net.bosai.go.jp/. Accessed 1 May 2008.
Kobayashi, I., Tateishi, M., Uemura, T., 1993. Geological Map of Japan 1:50,000, Izumozaki, Geological Survey of Japan (available digitally through GSJ, AIST Digital Geoscience Map G20–3).
Kobayashi, I., Tateishi, M., Kurokawa, K., Yoshimura, T, and Kato, H., 1989. Geological Map of Japan 1:50,000, Okanomachi, Geological Survey of Japan (available digitally through GSJ, AIST Digital Geoscience Map G20–4).
Kobayashi, I., Tateishi, M., Yoshimura, T., Ueda, T., and Kato, H., 1995. *Geological Map of Japan 1:50,000, Kashiwazaki*, Geological Survey of Japan (available digitally through GSJ, AIST Digital Geoscience Map G20-3)
Koketsu, K., Miyake, H., Hikima, K., 2007. Source inversion for the 2007 Chuetsu–oki, Japan, earthquake: a case of difficulty determining the source fault plane. Eos Transactions AGU 88 (52), S54A-05 Suppl. Abstract.
Kokusai Kogyo, 2007. Aerial photo interpretation of earthquake damage from the 2007 Niigata Chuetsu–oki Earthquake. consultant report Kokusai Kogyo Co., Ltd, Japan http://www.kkc.co.jp/social/disaster/200707_nigata/parts_tuika/gaikyozu.pdf (in Japanese), Accessed 1 May 2008.
Kyoji, S., Hiroshi, F., Fawu, W., Gonghu, W., 2005. Landslide triggered by 2004 Niigata Prefecture Earthquake and the sliding mechanism of the rapid landslides occurred within the past landslide masses. *Disaster Prevention Research Institute Annuals*, Kyoto University, 48A, pp. 171–189.
Lee, C.-T., Huang, C.-C., Lee, J.-F., Pan, K.-L., Lin, M.-L., Dong, J.-J., 2008. Statistical approach to earthquake-induced landslide susceptibility. Engineering Geology 100, 43–58.
Meunier, P., Hovius, N., Haines, J.A., 2008. Topographic site effects and the location of earthquake induced landslides. Earth and Planetary Science Letters 275, 221–232.
Milne, J., 1885. Seismic experiments. Transactions Seismological Society of Japan 8, 1–82.
Miyake, H., Koketus, K., Hikima, K., Shinohara, M., Kanazawa, T., 2010. Source Fault of the 2007 Chuetsu–oki, Japan, Earthquake. Bulletin of the Seismological Society of America 100 (1), 384–391.
Morton, D.M., Campbell, R.H., Jibson, R.W., Wesson, R.L., Nicholson, C.C., 1989. Ground fractures and landslides produced by the July 8, 1986, North Palm Springs Earthquake. In: Sadler, P.M., Morton, D.M. (Eds.), Landslides in a Semi-Arid Environment: Riverside, California, Inland Geological Society, vol. 2, pp. 183–196.
Nishimura, T., Tobita, M., Yarai, H., Amagai, T., Fujiwara, M., Une, H., Koarai, M., 2008. Episodic growth of fault-related fold in northern Japan observed by SAR interferometry. Geophysical Research Letters 35, L13301. doi:10.1029/2008GL034337.
NRI ESDP, 2007. Source process of the 2007 Niigata-ken Chuetsu–oki Earthquake derived from near-fault strong motion data. National Research Institute for Earth Science and Disaster Prevention. http://www.k-net.bosai.go.jp/k-net/topics/chuetsuoki20070716/inversion/ksw_ver070816_NIED_Inv_eng.pdf. Accessed 1 May 2008.
Omote, S., Miyahe, A., Narahashi, H., 1977. Maximum ground acceleration in the epicentral area — field studies on the occasion of the Ohita Earthquake, Japan of April 21, 1975. Bulletin: International Institute of Seismology and Earthquake Engineering 15, 67–82.
Papadopoulos, G.A., Plessa, A., 2000. Magnitude–distance relations for earthquake-induced landslides in Greece. Engineering Geology 58, 377–386.
Parise, M., Jibson, R.W., 2000. A seismic landslide susceptibility rating of geologic units based on analysis of characteristics of landslides triggered by the 17 January, 1994 Northridge, California earthquake. Engineering Geology 58 (3–4), 251–270.
Rodríguez, C.E., Bommer, J.J., Chandler, R.J., 1999. Earthquake-induced landslides: 1980–1997. Soil Dynamics and Earthquake Engineering 18, 325–346.
Sato, H., 2007. GIS analysis on the slope failures triggered by the Niigataken Chuetsu–oki earthquake in 2007. 4 pp Geographical Survey Institute of Japan, Disaster Research Report http://cais.gsi.go.jp/Research/geoinfo/slopefailuresChuetsu-oki.pdf (in Japanese), Accessed 1 May 2008.
Sitar, N., Clough, G.W., 1983. Seismic response of steep slopes in cemented soils. Journal of Geotechnical Engineering 109 (2), 210–227.
Takenaka, H., Yamamoto, Y., Yamasaki, H., 2007. High-resolution source imaging of the 2007 Niigataken Chuetsu–oki earthquake from dense strong-motion networks: focus on the first 5 seconds of the rupture process. Eos Transactions AGU 88 (52), S31A-0208 Suppl. Abstract.
Takenaka, H., Yamamoto, Y., Yamasaki, H., 2009. Rupture process at the beginning of the 2007 Chuetsu-oki, Niigata, Japan, earthquake. Earth, Planets, Space 61, 279–283.
Takeuchi, K., Yoshimura, T., and Kato, H., 1996. Geological Map of Japan 1:50,000, Kakizaki, Geological Survey of Japan (available digitally through GSJ, AIST Digital Geoscience Map G20–4).
Tazaki, K., Kimuar, S., Yoshimura, T., Akai, J., Fyfe, W.S., 1989. Clay–organic complexes as a cementing agent in the Arahama Sand Dune, Japan. Clays and Clay Minerals 37 (3), 219–226.
TEPCO, 2008. Report on Analysis of Observed Records at Kashiwazaki–Kariwa Nuclear Power Plant During the Niigata Chuetsu–oki Earthquake, 2007. http://www.tepco.co.jp/en/press/corp-com/release/betu07_e/images/070719_01.jpg. Accessed 15 September 2008.
Tobita, T., Ghayamghamian, M.R., Kang, C.-C., Iai, S., 2007. Preliminary report of the July 16, 2007 Niigata prefecture Chuetsu Offshore Japan Earthquake. Disaster Prevention Research Institute, Kyoto University, Japan, Vers. 1.2 http://geo.dpri.kyoto-u.ac.jp/research/2007Niigata-Chuetsu-Oki/2007-Niigata-Chuetsu-oki-v11.pdf. Accessed 16 September 2008.
Toda, S., 2007. 2007 Mw=6.6 Niigata Chuetsu–Oki earthquake ruptured on a fault strongly unclamped by the 2004 Mw=6.6 Niigata Chuetsu shock. Eos Transactions AGU 88 (52), S31B-1301 Suppl. Abstract.
USGS, 2007. United States Geological Survey Earthquake Hazards Program. Earthquake Summary: Magnitude 6.6 Earthquake Near the West Coast of Honshu, Japan http://earthquake.usgs.gov/eqcenter/eqinthenews/2007/us2007ewac/#summary. Accessed 1 May 2008.
Varnes, D.J., 1978. Slope movement types and processes. Landslides, analysis and control. In: Schuster, R.L., Krizek, R.J. (Eds.), Transportation Research Board Sp. Rep. No. 176: Nat. Acad. of Sciences, pp. 11–33.
Wang, X., Nie, G., Wang, D., 2010. Research on relationship between landslides and peak ground accelerations induced by Wenchuan earthquake. Chinese Journal of Rock Mechanics and Engineering 29, 82–89.
Wasowski, J., del Gaudio, V., Pierri, P., Capolongo, D., 2002. Factors controlling seismic susceptibility of the Sele valley slopes: the case of the 1980 Irpinia earthquake re-examined. Surveys in Geophysics 23, 563–593.
Wilson, R.C., Keefer, D.K., 1985. Predicting aerial limits of earthquake-induced landsliding. In: Ziony, J.I. (Ed.), Evaluating Earthquake Hazards in the Los Angeles Region — An Earth-Science Perspective: USGS Professional Paper, 1360, pp. 316–345.
Winkler, T., Meguro, K., Yamazaki, F., 1995. Response of rigid body assemblies to dynamic excitation. Earthquake Engineering and Structural Dynamics 24, 1389–1408.
Yamagishi, H., Iwahashi, J., 2007. Comparison between the two triggered landslides in Mid-Niigata, Japan by July 13 heavy rainfall and October 23 intensive earthquake in 2004. Landslides 4 (4), 389–397.
Yamagishi, H., Tomizawa, Y., Nakasuzi, A., Nozaki, Y., Hirano, Y., Nakagawa, W., Yasuda, T., Tanase, A., Sudou, H., Mito, S., Nagano, H.O., Ono, M., Yasuda, Y., Hama, Y., 2007. Urgent report of the 2007 Niigataken Chuetsu–oki earthquake disaster. Journal of the Japan Society of Engineering Geology 48 (4), 192–202 (in Japanese).
Yim, C.-S., Chopra, A.K., Penzien, J., 1980. Rocking response of rigid blocks to earthquakes. Earthquake Engineering and Structural Dynamics 8, 565–587.
Yin, Y., Wang, F., Sun, P., 2009. Landslide hazards triggered by the 2008 Wenchuan earthquake, Sichuan, China. Landslides 6 (2), 139–151.